Gut-Liver physiomimetics reveal paradoxical modulation of IBD-related inflammation by short-chain fatty acids

Martin Trapecar[1], Catherine Communal[1], Jason Velazquez[1], Christian Alexander Maass[1,2], Yu-Ja Huang[1], Kirsten Schneider[1], Charles W. Wright[1], David Trumper[3,4], Linda G. Griffith[1,3,5]*

Affiliations:
[1]Department of Biological Engineering, Massachusetts Institute of Technology, Cambridge, MA, USA.
[2]Certara U.K., Quantitative Systems Pharmacology, Sheffield, UK
[3]Department of Mechanical Engineering, Massachusetts Institute of Technology, Cambridge, MA, USA.
[4]Research Laboratory of Electronics, Massachusetts Institute of Technology, Cambridge, MA, USA.
[5]Center for Gynepathology Research, Massachusetts Institute of Technology, Cambridge, MA, USA.

*Correspondence to: griff@mit.edu

Abstract: Association between the microbiome, IBD and liver diseases are known, yet cause and effect remain elusive. By connecting human microphysiological systems of the gut, liver and circulating Treg/Th17 cells, we modeled progression of ulcerative colitis (UC) ex vivo. We show that microbiome-derived short-chain fatty acids (SCFA) may either improve or worsen disease severity, depending on the activation state of CD4 T cells. Employing multiomics, we found SCFA reduced innate activation of the UC gut and increased hepatic metabolism. However, during acute T cell-mediated inflammation, SCFA exacerbate CD4 T cell effector function leading to gut barrier disruption and liver damage. These paradoxical findings underscore the emerging utility of human physiomimetic technology to study causality and temporal facets of gut-liver axis related diseases where animal models leave ambiguity.

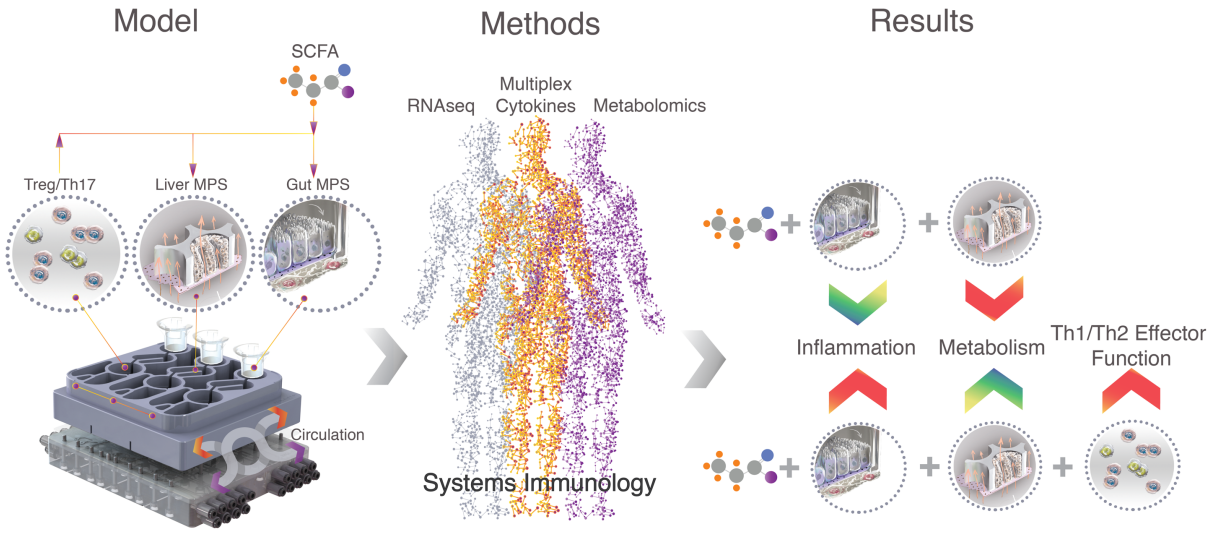

The gut-liver axis is a highly connected system whose roles include processing of gut-derived products, regulation of metabolic homeostasis and stability of systemic immune function (*1*). Thus significant correlations exist between inflammatory bowel disease (IBD), like ulcerative colitis (UC) or Crohn's disease (CD), and inflammatory liver diseases such as autoimmune hepatitis or primary sclerosing cholangitis (PSC) (*2*). Risk to develop autoimmune liver disease is increased in patients with IBD and up to 80% of patients with PSC have concurrent UC (*3*). The manifestations of these interconnected pathologies are relatively well described, yet the "cause and effect" paradox remains to be solved.

A common feature of IBD and extra-intestinal complications is the influx of destructive immune cells (*4*). Most forms of hepatitis show initial infiltration of T cells via the portal vessels and are crucial for the development of chronic liver inflammation (*5*). At the heart of the balance between autoimmunity and tolerance lie CD4 regulatory T cells (Tregs), producing TGF- β (*6*), and Th17 cells (Th17s) releasing the cytokines IL-17 and IL-22 (*7*). Treg/Th17 disbalance has been extensively reported in both IBD (*8, 9*), autoimmune liver diseases (*10*) as well as organ rejection (*11*). Furthermore, plasticity of both Tregs and Th17s allows them to transition into more acute inflammatory CD4 Th1/Th2 hybrid subtypes under acute conditions via antigen and antigen-independent activation. UC is associated with a Th2/ Th17 phenotype and ample production of IL-13, while CD is connected with Th1/Th17 effector response (*12-14*).

While many drivers of autoimmunity and inflammation in the gut-liver axis remain unknown, they are influenced by the microbiome. Short-chain fatty acids (SCFA) are microbial metabolites derived from microbial fermentation of fiber in the colon (*15*). The most abundant SCFA are acetate, propionate and butyrate and their concentration (up to 120 mM) is linked to SCFA producing bacterial phyla (*16, 17*). SCFA have been shown to exert a variety of beneficial effects on the host (*15, 18*). Among these are increased gut barrier function, liver glucose metabolism, reduction of IBD associated symptoms and promotion of immune tolerance. Contrary to the latter findings, accumulating data shows SCFA to enhance both CD4 (*19-21*) and CD8 (*22, 23*) T cell effector function. Several animal and human trials found SCFA to either lack any therapeutic efficacy or to exacerbate inflammation (*16, 17, 24-27*). Conflicting results suggest the function of SCFA to be context and disease severity dependent, thus their role in T cell activation and metabolism under conditions of gut-liver inflammation in humans demands urgent clarification.

Recently-developed *in vitro* physiomimetic technology, in combination with systems immunology, offers new possibilities for illuminating mechanisms in multi-organ inflammatory diseases by modeling complex interactions with multiple interconnected human microphysiological systems (MPSs) (*28*). MPSs are *in vitro* models that are both complex - comprising multiple cell types, specialized microenvironments, and perfusion – and yet reductionist, as they capture only the most salient features of *in vivo* organ behavior required to model the physiological process in question. We previously developed a physiomimetic platform technology that supports long-term (weeks) integrated co-culture of up to 10 fluidically-communicating MPSs, featuring individually-addressable on-board microfluidic pumps compatible with highly lipophilic compounds such as steroid hormones (*29-31*). Here, we use a new iteration of the platform designed to model the gut-liver-immune axis by connecting a gut MPS of UC (primary human UC epithelium, dendritic cells and macrophages) with a liver MPS (healthy human hepatocytes and Kupffer cells) and circulating Treg/Th17 cells. By measuring gene transcription, cytokines and metabolomic changes during different modes of interaction, we gained new insight on the connectedness between UC, liver function and SCFA in an all-human model. While SCFA may reduce innate immune activation of primary tissue, they may also increase the effector function of activated CD4 T cells and thus exacerbate acute UC inflammation and raise the risk of liver injury.

Gut MPS of ulcerative colitis donor, but not healthy donor, directs polarization of Treg/Th17 cells into Th1/Th2 cytokine producing effector subtypes in absence of SCFA

First, in the absence of SCFA and under static conditions off-platform, we compared baseline behaviors of healthy and UC gut MPSs on the basis of disease status, immune activation, and growth characteristics through (i) differential gene expression analysis of the epithelia; (ii) immunofluorescent imaging; and (iii) cytokine production and concomitant ability to disrupt Treg/Th17 balance. Gut MPSs were established by seeding equal numbers of epithelial cells from a UC donor and from a non-diseased control on separate transwell membranes, and then attaching peripheral blood mononuclear cells (PBMC)-derived macrophages and dendritic cells on the basolateral side of the membrane after monolayer differentiation. All experiments were conducted in a slight modification of culture medium which had previously been tailored for physiological inflammatory responses of the human liver MPS, in which the extreme supra-physiological concentrations of cortisol and insulin typically used to maintain CYP450 levels in primary hepatocyte cultures were reduced to concentrations within the physiological range (*30*).

After 4 days of epithelial coculture with innate immune cells, gene expression assayed in epithelia harvested from the apical side of replicate transwell co-cultures showed classic hallmarks of UC disease phenotype when UC epithelia were compared to the control epithelia using pathway enrichment based on GEO (Fig.1A). Further, gene ontology (GO) enrichment analysis (Fig.1B) showed a strong upregulation of pathways associated with innate immune activation, apoptotic signaling and EGF activity in the UC epithelia. Pathway analysis based on KEGG (Fig.1C) revealed increased cancer-related signaling through MAPK and PI3K-Akt pathways, which indicates increased cancerous neoplasticity and possible progression into carcinoma. Morphologically, epithelia from both donors formed confluent monolayers (Fig.1D) and exhibited comparable transepithelial resistance (Fig.1E). However, monolayers of UC, but not healthy gut MPSs, showed enlargement of hyperchromatic nuclei and irregular actin fragmentation, indicators of IBD dysplasia (Fig.1E) (*32*). These morphological findings are consistent with observation that differentially- expressed genes (Fig.1B,C) include those associated with regulation of actin, focal adhesions and cell junction, which are indicative of IBD-associated remodeling (*33*).

We next compared the inflammatory potential of the UC vs. control donors on the basis of cytokine production by the individual epithelium alone, epithelium in coculture with macrophages/dendritic cells (i.e. gut MPS) and during gut MPS coculture with PBMC derived Tregs and Th17 cells (ratio of 2:1) from the same donor as the antigen-presenting cells. Analysis of 41 cytokine concentrations in the basal medium after 48 h by principal component analysis clearly distinguishes individual donors in all 3 conditions based on cytokine/chemokine production (Fig.1F), where 59% of the variability was explained by the presence or absence of Treg/Th17 cells and 18% by the donor. Mean values of the majority of measured cytokines/chemokines were more highly expressed by the UC donor regardless of the coculture condition (Fig.1G, Fig. S1A,B). Interestingly, VEGF concentrations were persistently higher in all conditions with the healthy donor despite VEGF's known association with UC. This can be explained by a higher expression of VEGF receptors on UC epithelium and increased receptor-mediated VEGF internalization and degradation (Fig.S1C) thus reducing measurable free autocrine VEGF (*34*). Despite twice the number of Tregs over the number of Th17s, $CD4^+$ T cells began to polarize in their cytokine production toward a mix of Th1, Th2, Th17 cytokine producing cells in coculture with the UC gut MPS. The UC donor MPS induced T cell production of IL-4, Il-5, IL-13, TNF-α and interferons (Fig.S1A). This set of increased inflammatory cytokines coincides with previous reports showing UC epithelia to predominantly induce Th2/Th17 conditions (*12*). The Treg/Th17 balance remained intact in coculture with the healthy gut MPSs as indicated by the preserved Treg production of TGF-β1 and -β2 and low IL-17A release (Fig. S1B). The machine learning algorithm Random Forests was able to predict the MPS donor with 100% accuracy when

cocultured with Treg/Th17 cells (Fig.S1D); the most predictive factors were the pleiotropic lymphocyte attractants MIP-1β, MDC, and MCP-3 (Fig.1F). Both epithelial donors share the HLA alleles HLA A*02, B*51, DQA1*04, DQB1*06 and DRB1*03 which taken together with the physical separation of the epithelium and co-cultured underlying immune cells via 0.4μm microporous membranes, makes the rapid activation of CD4 T cells due to greater donor-mismatch highly unlikely.

Throughout the rest of the study, the UC gut MPS was used to further clarify the interaction of SCFA, inflamed gut tissue, liver MPS, and circulating T cells.

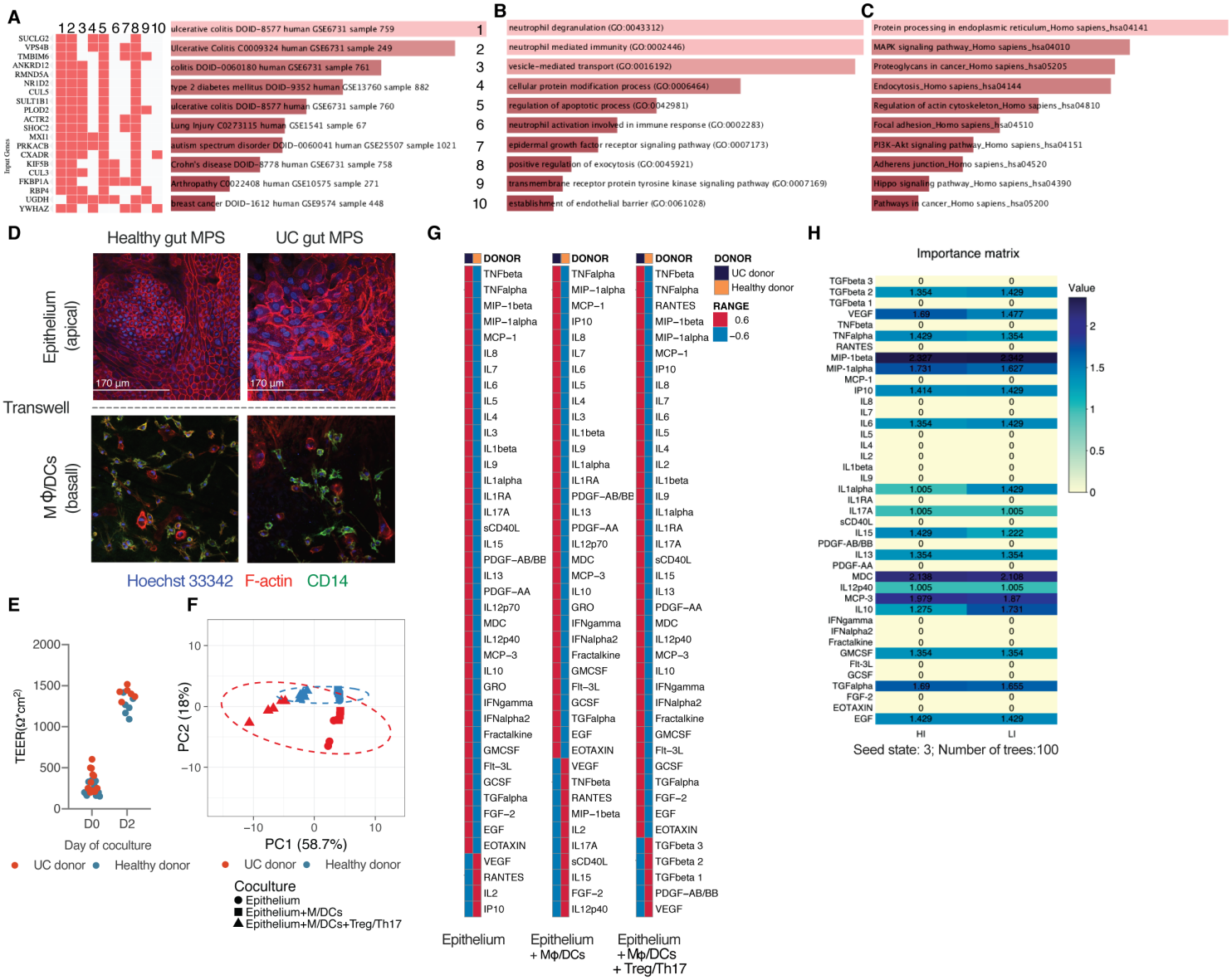

Fig.1 Coculture of the UC gut MPS with Treg/Th17 cells leads to increased production of Th1 and Th2 inflammatory cytokines Differential gene expression pathway enrichments in UC gut MPS as compared to healthy control MPS based on GEO disease related pathway enrichments (A), GO Biological process terms (B) or KEGG (C). (A-C) Data represent averages of 3 biological replicates. (D) Representative confocal images of gut MPS from the healthy gut MPS (left) and UC gut MPS (right). Top: epithelial monolayers seeded on the apical side of transwell membranes. Bottom: Cocultured macrophages and dendritic cells seeded on the basal side of transwell membranes (E) Representative TEER values of UC and healthy gut MPS at day 0 of gut MPS development and at day 2. (F) Representative PCA of multiplexed cytokines/chemokines released by each donor's epithelium alone, their corresponding MPS, and MPS interacting with Treg/Th17 cells. (G) Collapsed heatmaps based on means representative of 3-5 biological replicates indicating Z scores of cytokines/chemokines expressed under each condition as described under (F). (H) Importance matrix derived from random forest analysis of cytokines/chemokines released by gut MPSs in coculture with Treg/Th17s. For actual concentration values of individual cytokines/chemokines measured consult Figure.S1.

Bioaccessible SCFA lead to enrichment in metabolic pathways and reduction of inflammatory pathways in the UC gut MPS

As influence of SCFA on healthy epithelium has been described before (*15*), we focused on investigating its effects on the inflamed UC tissue and MPS. First, we investigated the interaction of SCFA and UC epithelium under static conditions alone without the presence of antigen presenting cells. Acetate, propionate and butyrate in a physiological molar ratio of 6:2:2 (*35*) at a total combined concentration of 20mM were added to the apical media of UC epithelial monolayers in transwell inserts. After 4 days of culture (with a media and SCFA change at 48 hr), tissue was harvested, RNAseq performed, and differential gene expressions established against untreated control groups (Fig.2 A,B). KEGG pathway enrichment analysis showed a significant upregulation of Foxo and the PPAR signaling pathway (Fig. 2B), mainly PPAR-α/δ, that drives glycerolipid metabolism upon fatty acid stimulation and ketone body production (*36*). Concurrently, cell cycle pathways were down regulated as well as genes associated with proteoglycan synthesis in cancer. In vitro studies have shown SCFA to inhibit proliferation of cancer cell lines; in addition reduction in butyrate-producing bacteria is linked to both colorectal cancer development and progression (*37*). Further analysis based on different databases (Fig.S2) shows strong global upregulation of fatty acid metabolism pathways and suppression of TNF, NF-kappa B and chemotactic inflammatory pathways.

Next, we established the bioaccessibility and clearance of SCFA (20mM) by the UC gut MPS with macrophages and dendritic cells under basolateral circulation at a flow rate of 1µL/s. Over the course of 48 hours, 54% of butyrate was consumed by the UC gut MPS while the majority of acetate (96%) and propionate (82%) passed the gut barrier into the basal compartment (Fig.2C, Fig.S3). These results correlate with human clinical data that show butyrate serves as the primary energy source of colonocytes and that in average only 50% of butyrate reaches the portal vein (*35*). As a result, the molar ratio of SCFA in portal blood switches to 7:2:1. Epithelial barrier was maintained throughout the time course (Fig.2D). Concurrently, epithelial tissue was harvested at 4 h, 8 h, 24 h and 48 h post SCFA application to identify time dependent changes in gene expression and to validate SCFA effects seen under Figure 2B. Principal component analysis of expressed genes showed significant changes throughout the time course (Fig.2E). Further analysis repeatedly indicated downregulation of UC gut MPS genes governing cell cycle and WNT signaling through FoxO as reported *in vivo* (*38*), as well as upregulation of hormone receptor activity, expression of integral membrane proteins and ECM remodeling. Moreover, in the coculture of the inflamed UC epithelium with antigen-presenting cells, SCFA downregulated inflammatory NF-kappa B signaling pathways as seen with the epithelium alone (Fig.2B), which confirms previous reports on anti-inflammatory potential of SCFA (*15*).

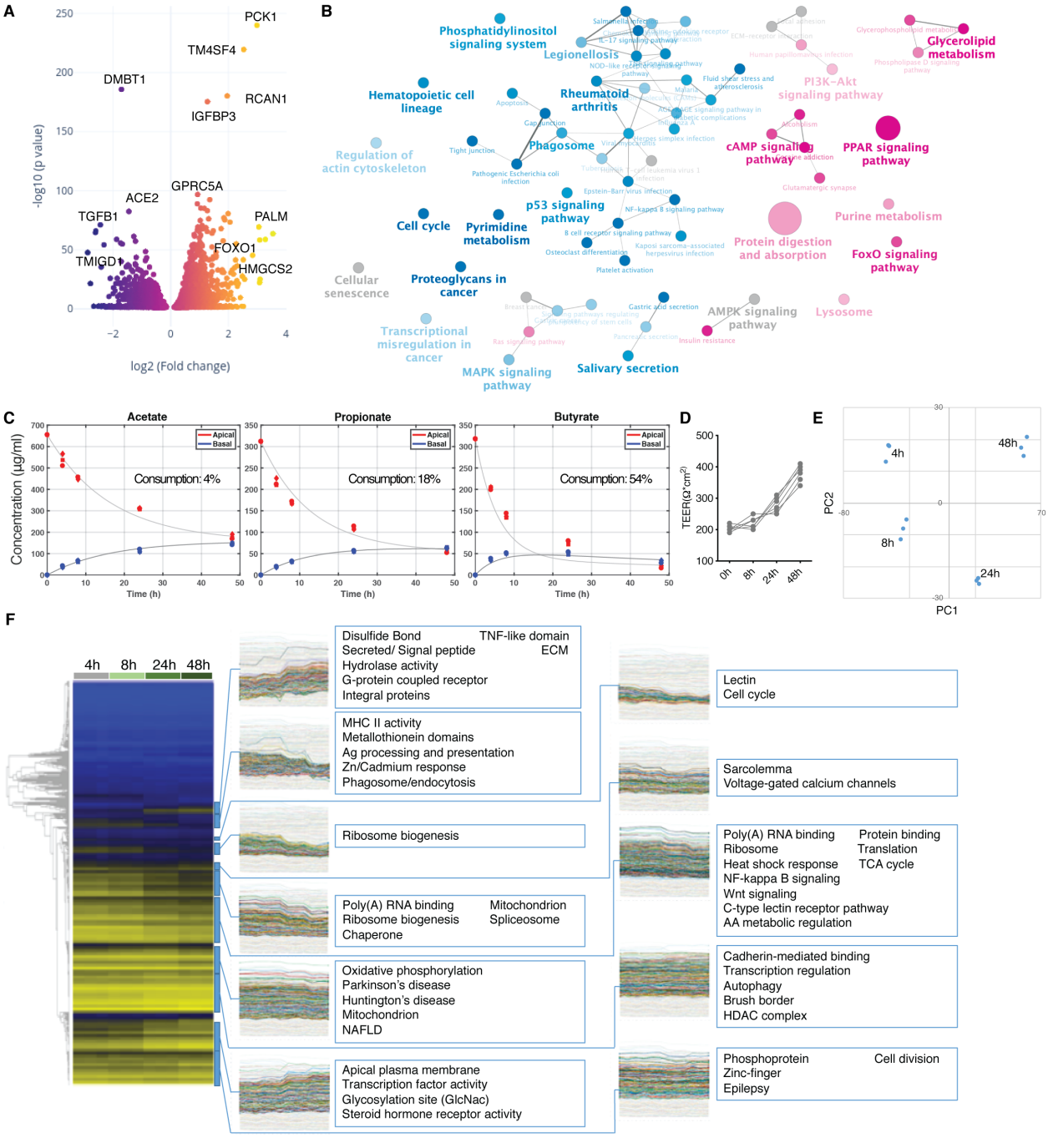

Fig.2 Bioaccessible SCFA affect gene expression of UC epithelium and the UC gut MPSs (A) Volcano plot of differentially expressed genes (DEG) in monolayers of UC epithelium with SCFA over controls without. (B) Network of enriched (magenta) and suppressed (blue) KEGG pathways based on DEG shown under (A). (C) Apical and basal concentrations of acetate, propionate and butyrate over 48h in UC gut MPSs upon an initial apical total SCFA concentration of 20mM. Consumption of each SCFA by the epithelium is shown as percent loss in corresponding plots. Each time point was measured in 3 biological replicates. (D) Representative TEER values of gut MPSs cultured with 20mM of SCFA. (E) PCA analysis of changes in epithelial gene expressions at each time point shown under (C). (F) Epithelial tissue from each time point shown under (C) was harvested for RNAseq analysis. Left: Heat-maps with gene-level dendrograms. Right: Clades from the gene-level hierarchical clustering with gene expression time-course representations of each gut MPS interacting with SCFA. Each time point represents 3 biological replicates.

Interaction between SCFA, gut and liver MPSs results in decreased innate inflammation of the gut MPS and increased hepatic metabolism

Having established that apical SCFA are transported across the colonic epithelial barrier, partially metabolized by the colonic epithelia, and reduce signatures of inflammation of UC epithelia compared to controls without SCFA, we next used a new iteration of our physiomimetic platform, the 3XGL (3 modules of "gut-liver" per platform; Fig.S3A), to investigate the effects of SCFA on the gut-liver axis. We focused initial experiments on behaviors of the gut-liver axis in the absence and presence of SCFA without adaptive immune cells, using the gut and liver MPSs connected at recirculating flow rates of 30 ml/day. Integration of gut and liver MPSs significantly affects their individual phenotypes and gene expression (Fig.S4A,B) in accordance with our previous observations during interaction of a CaCo-2 cell based MPS with the liver MPS (*30, 31*). The most notable effects were decreased glycolysis and increased CYP450 and steroid hormone synthesis of the gut MPS (Fig.S4A) and increased CYP450 activity with downregulation of inflammatory pathways in the liver MPSs (Fig.S4B). Decreased innate activation of the UC gut MPS had an anti-inflammatory effect on the liver MPS, linking the state of gut activation to liver homeostasis. UC is tightly connected to liver PSC, and clinical data show that even after liver transplantation, UC and gut inflammation pose an increased risk for PSC recurrence (*39*).

We next performed a 4 day interaction experiment between gut and liver MPSs with the addition of 20 mM of total SCFA into the apical gut media. On day 4 (after an interim medium and SCFA refreshment on day 2), media were collected for cytokine and metabolomic analyses and tissue harvested for RNAseq (Fig. 3A-F). During interaction, SCFA were both adsorbed and metabolized by the gut MPS and further metabolized by the liver MPS (Fig S5B) at similar rates when measured in day 2 as well as day 4 media. Liver clearance rates for SCFA, derived with PBPK models using concentrations of SCFA measured in the gut basal compartment during interaction (Fig S5A) and gut MPS absorption and metabolism data in isolation (Fig 2C), show a pattern consistent with known in vivo clearance: near-complete clearance of butyrate, intermediate clearance of propionate, and considerably lower clearance of acetate. Gene expression clustering clearly separates the gut MPS epithelial tissue from liver MPS samples and validates the presence of tissue specific genes (Fig.S5B). SCFA induced significant changes in both MPS compared to control interactions (Fig3A,C). During gut-liver interaction, changes in UC tissue upon addition of SCFA are highly consistent with changes observed in isolation studies: upregulation of PPAR, hormone synthesis pathways and suppression of NF-kappa B signaling based on KEGG was observed (Fig.3B). Moreover, pathways of the glutaminergic synapse were enriched after addition of SCFA due to increased expressions of glutamate metabolism genes with implied neurotropic effects of SCFA. Epithelial TEER measurements of both gut-liver and gut-liver-SCFA interaction groups were comparable to the control in isolation and were maintained in the in vivo physiological range between 100-400 Ohms/cm^2 (*40*). Hepatic albumin production increased throughout this interaction (Fig.S5C,D,E). SCFA added to the apical compartment of the gut MPS, absorbed, and transported to liver MPS induced upregulation of several metabolic pathways of the liver MPS in accordance with observations in vivo (*41*), including gluconeogenesis, retinol and tyrosine metabolism as well as bile acid synthesis and secretion, as confirmed by KEGG analysis (Fig.4D).

Addition of SCFA to the apical gut MPSs in the gut-liver interaction condition had a dramatic effect on production of cytokines released into the common medium. Cytokine analysis of the shared common medium showed significant reduction of inflammatory mediators in the SCFA treated group (Fig.3E, Fig.S6A,B).

Most predictive parameters distinguishing SCFA-treated interaction group from the non-treated were reduced PDGF, IL-9, GRO and MDC based on random forest analysis (Fig.S6C).

Reduced secretion of the chemoattractants GRO and MDC correlates to decreased enrichment of innate immune pathways.

Global metabolomic discovery of the common media from samples collected at day 4 for the +/- SCFA conditions in gut-liver interaction indicated enrichment in fatty acid metabolism, ketone body synthesis and increased creatine metabolism (Fig.3F) related to increased PPAR signaling in the presence of SCFA (*36*), consistent with gene expression results for UC epithelia in isolation (Fig 2B). Glucose consumption and conversion into lactate was higher in the gut-liver-SCFA interaction at day 2 but not at day 4 (Fig.S7A) which implies early increased global metabolic activity supported by the increase of TCA intermediate aconitate (Fig.S7B). Ketone bodies are produced by the liver under fasting condition through conversion of SCFA and by conversion of butyrate in the colon (*42, 43*). In our system, production of ketone bodies without SCFA stems predominantly from the liver MPS and is increased by SCFA (Fig.S7C). The gene-metabolite integration of overlapping gene and metabolomic enrichments for each MPS reveals common as well as individual metabolic pathways of both tissues (Fig.3G,H). SCFA induced glycerophospholipid and glycersphyngolipid metabolism are more prevalent in the gut MPS. They are tightly connected to gut health by promotion of cytokine synthesis and cell structure integrity (*44*). Fatty acid, butanoate and propionate metabolism was highly induced in the liver MPS confirming liver metabolism of these SCFA.

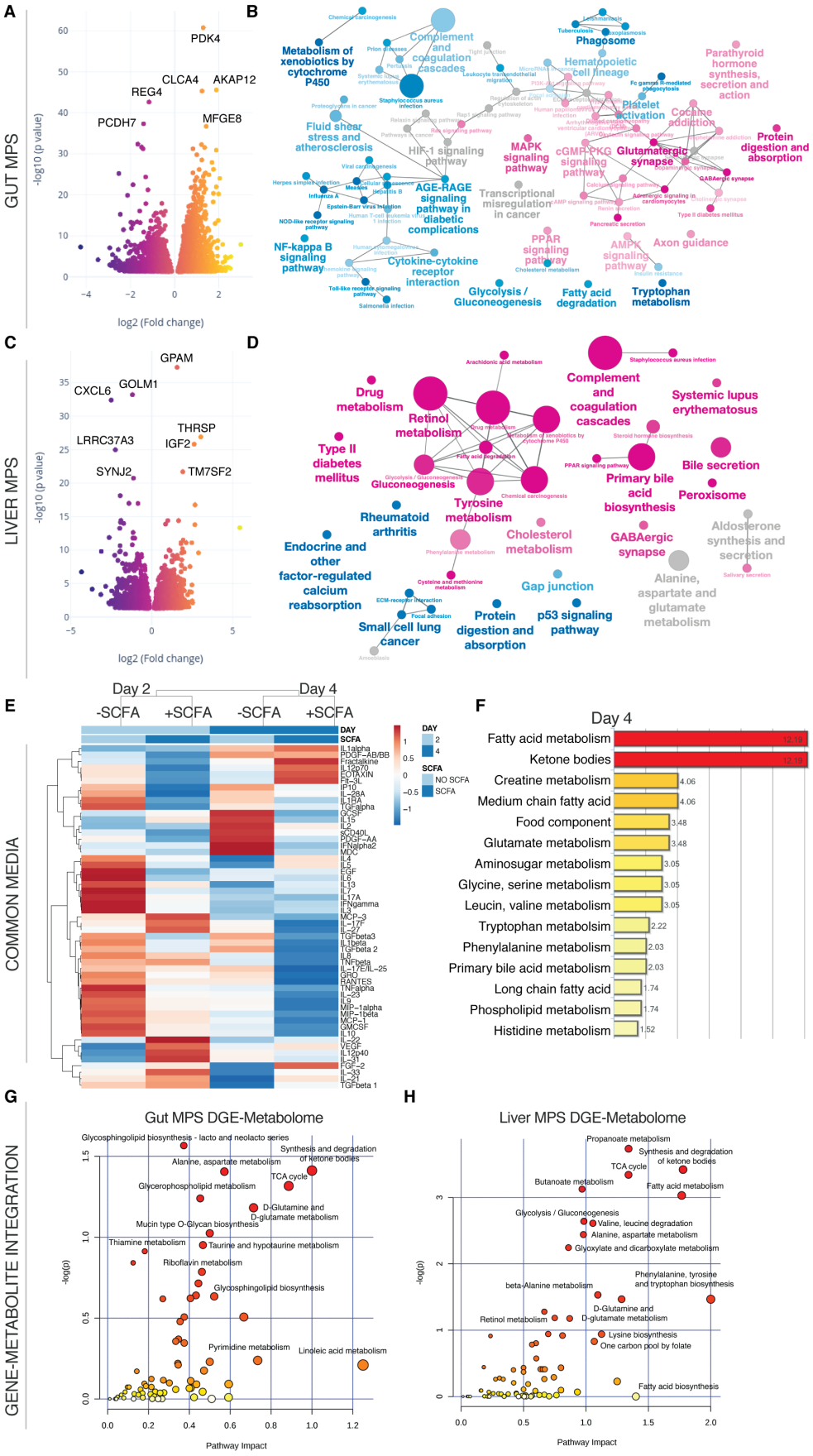

Fig.3 SCFA reduce innate immunity of the UC gut MPS and beneficially affect hepatic metabolism during interaction (A,C) Volcano plots of DEG in the gut MPS (A) and the liver MPS (C) in presence or absence of SCFA. (B,D) Network of enriched (magenta) and downregulated (blue) pathways based on KEGG in gut MPS (B) or liver MPS (D). (E) Clustered heatmap of multiplexed cytokines/chemokines present in circulating common media at day 2 and 4 during gut-liver MPS interaction +/- SCFA. For concrete concentrations of measured proteins and their importance consult Fig.S6. (F) Significantly enriched metabolic pathways based on quantification of metabolites found in the common medium at day 4 of gut-liver-SCFA interactions. (G,H) Integration of significantly upregulated genes in the UC gut MPS (G) or liver MPS (H) during interaction with SCFA and enriched metabolites found in the common medium at day 4. Pathway impact score is shown on the x-axis and statistical significance on the y-axis. All data represents 3 biological replicates.

Inclusion of Treg/Th17 cells during gut-liver interaction leads to UC triggered acute T cell mediated inflammation and autoimmune hepatitis

We introduced Treg/Th17 cells in a 2:1 ratio and equal numbers into all compartments of the platform with circulation-enabled transport between MPSs. Gene cluster analysis indicated partial engraftment of Treg/Th17 cells within the liver tissue itself based on the expression of FOXP3, ICOS and CD28 (Fig.S5B). As observed in studies of gut MPSs in isolation, the UC gut MPSs induced a high degree of activation of added CD4 T cells, which led to decreased gut barrier function and reduced liver albumin secretion (Fig.SC,D,E) . In parallel 4-day interaction studies where the same donors of liver hepatocytes, Kupffer cells and PBMCs were used as in this experiment, but with the characterized healthy epithelium donor, Th1/Th2 activation was largely absent and gut barrier as well as liver albumin production preserved (manuscript in preparation).

The CD4 T cell-driven inflammation led to significant upregulation of interferon-induced genes in both tissues as compared to the control gut-liver interaction without lymphocytes (Fig.4A,C). Pathways associated with Th1/Th2 differentiation and IBD were highly enriched based on KEGG (Fig.4B) in the gut MPS with increased NOD signaling as well as reduction of lipid metabolism. NOD2 was the first gene associated with IBD and promotes Th17 differentiation (*45*). In response hepatic tissue showed strong enrichment of both Th17 and Th1/Th2 differentiation pathways (Fig.4D). In mice, blocking migration of intestinal effector T cells prevented hepatic allograft rejection establishing a clear link between the gut and autoimmune disease (*46*). A high correlation exists also between UC and autoimmune hepatitis with or without fibrotic PSC (*47*). In mice, T cells were shown to accumulate in the portal region of the liver and drive Th1-like autoimmune liver inflammation (*48*) while Th17 and Th2 CD4 T cells were associated with tissue fibrosis and injury (*49*).

Predictably, cytokine/chemokine concentration of inflammatory mediators, such as IFN-γ, TNF-α, IL-1α and RANTES, were strongly increased in the presence of activated lymphocytes at day 4 (Fig.4E). While fatty acid metabolism remained intact based on global metabolomic enrichments (Fig.4F), both glycolysis and purine metabolism increased at day 4. Acute inflammation of tissue is associated with a drastic shift in metabolism towards aerobic energy transformation including increased purinergic signaling (*50*) and glucose consumption (Fig.S7A) by T cells. This is in line with the observed enrichment of the mevalonate metabolism at day 4, which is a result of active T cell conversion of glucose to acetyl-CoA due to the Warburg effect (*51*). Gene-metabolite integration analysis also indicates strong upregulation of the pyrimidine and nicotinamide metabolism in both tissues (Fig.4G-H). A significant enrichment of sphingolipids was detected, which correlates to clinical data identifying sphingolipids as clinical markers of autoimmune hepatitis in patients' serum (*52*).

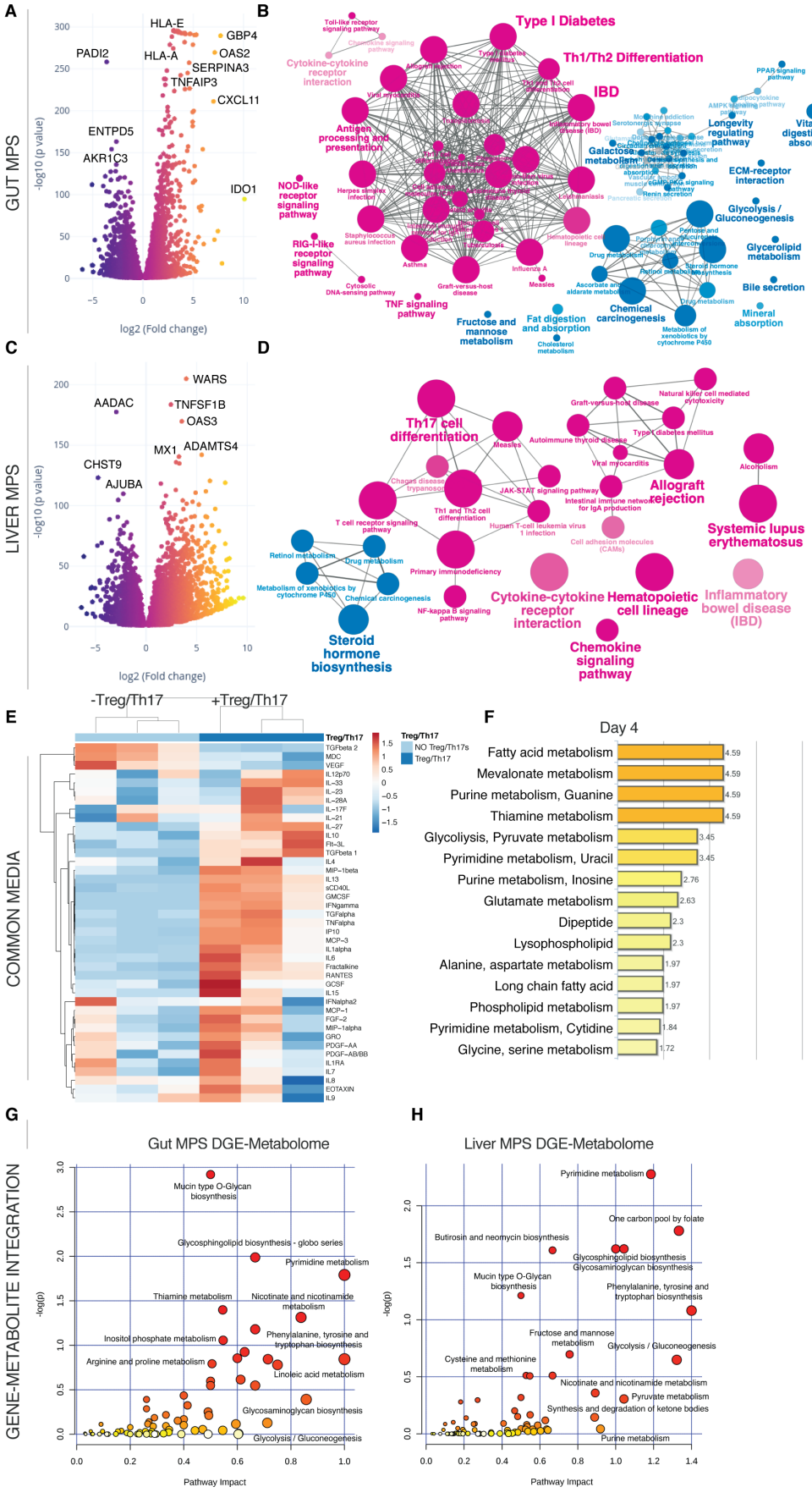

Fig.4 Inclusion of Treg/Th17 cells in the UC gut-liver MPS interaction leads to their conversion into inflammatory Th1/Th2 cells (A, C) Volcano plots of DEG in the gut MPSs (A) during interaction with the liver MPSs (C) in presence or absence of Treg/Th17 cells. (B, D) Network of enriched (magenta) and downregulated (blue) pathways based on KEGG in gut MPSs (B) or liver MPSs (D). (E) Clustered heatmap of multiplexed cytokines/chemokines present in circulating common media at day 4 during gut-liver MPS interaction +/- Treg/Th17 cells. (F) Significantly enriched metabolic pathways based on quantification of metabolites found in the common medium at day 4 of gut-liver-Treg/Th17 interactions. (G,H) Integration of significantly upregulated genes in the UC gut MPSs (G) or liver MPSs (H) during interaction with Treg/Th17 cells and enriched metabolites found in the common medium at day 4. Pathway impact score is shown on the x-axis and statistical significance on the y-axis. All data are derived from 3 biological replicates.

T cell mediated acute inflammation is exacerbated by SCFA, leading to hepatic failure and gut barrier disruption

As innate immune activation was reduced by SCFA in the inflamed gut MPSs as well as during interaction with the liver MPSs, we next added 20 mM of total SCFA into the apical gut medium in the model of acute CD4 T cell-mediated gut-liver inflammation. Compared to controls without SCFA, inflammation and tissue damage were surprisingly further amplified with their addition. The differential gene expression of the gut MPSs showed asymmetrical downregulation of homeostatic genes and further potentiation of genes related to immune activation (Fig.5A). NF-kappa B with TNF signaling pathways and pathways associated with systemic inflammation were strongly enriched in combination of mTOR activity (Fig.5B) and coinciding with further damage of the epithelial barrier (Fig.S5C,D), indicating irreparable tissue damage. While T cell-mediated inflammation prompted considerable reduction of TEER, addition of SCFA lead to complete barrier failure. Similarly, albumin production of the liver MPS stalled in both groups (Fig.S5E). This observation correlates with wide-ranging downregulation of major metabolic pathways (Fig.5D) and enrichment in MAPK related pathways.

Multiplex cytokine/chemokine analysis showed increased production of inflammatory cytokines when SCFA were added (Fig.5E, Fig.S8A,B). In particular IFN-γ, IL-5, IL-8, IL-10, and IL-13 were the most condition-predictive cytokines based on random forest analysis (Fig.S8C-E) which is indicative of both Th1 and Th2 expansion. Interestingly, several cytokine concentrations (e.g. IFN-γ and TNF-α) measured during this interaction were similar to reported levels in serum of patients with IBD (*53, 54*).

In the group with added SCFA, tryptophan conversion into kynurenate as part of the inflammatory IDO pathway was significantly higher as well (Fig.S9A). A similar trend was observed with the kynurenate downstream product quinolinate that serves as precursor of nicotinamide (Fig. S9B). The global metabolomic profile shows enrichments of ketone bodies similar to the gut-liver-SCFA interaction without Treg/Th17 cells (Fig.5F). Mevalonate and thiamine metabolism were further enriched during T cell-mediated inflammation and addition of SCFA. Both glucose consumption and production of pyruvate, lactate and aconitate were highest in the gut-liver-Treg/Th17-SCFA interaction group at day 2 but not day 4, which might be explained by increased tissue failure by that point (Fig.S7A). Increased lactate production indicated a metabolic switch into inflammation-driven aerobic metabolism. The gut MPS showed enriched glutathione metabolism over the controls without SCFA based on gene-metabolite integration while alanine, aspartate and glutamate metabolism were enriched in both gut and liver MPSs (Fig.5G,H). Glutamate metabolism is essential for T cell function under inflammation and its downstream product glutathione for reduction of oxidative stress (*55*). Furthermore, the liver MPSs showed significant enrichment in metabolism of histidine, a histamine precursor and vital inflammatory agent.

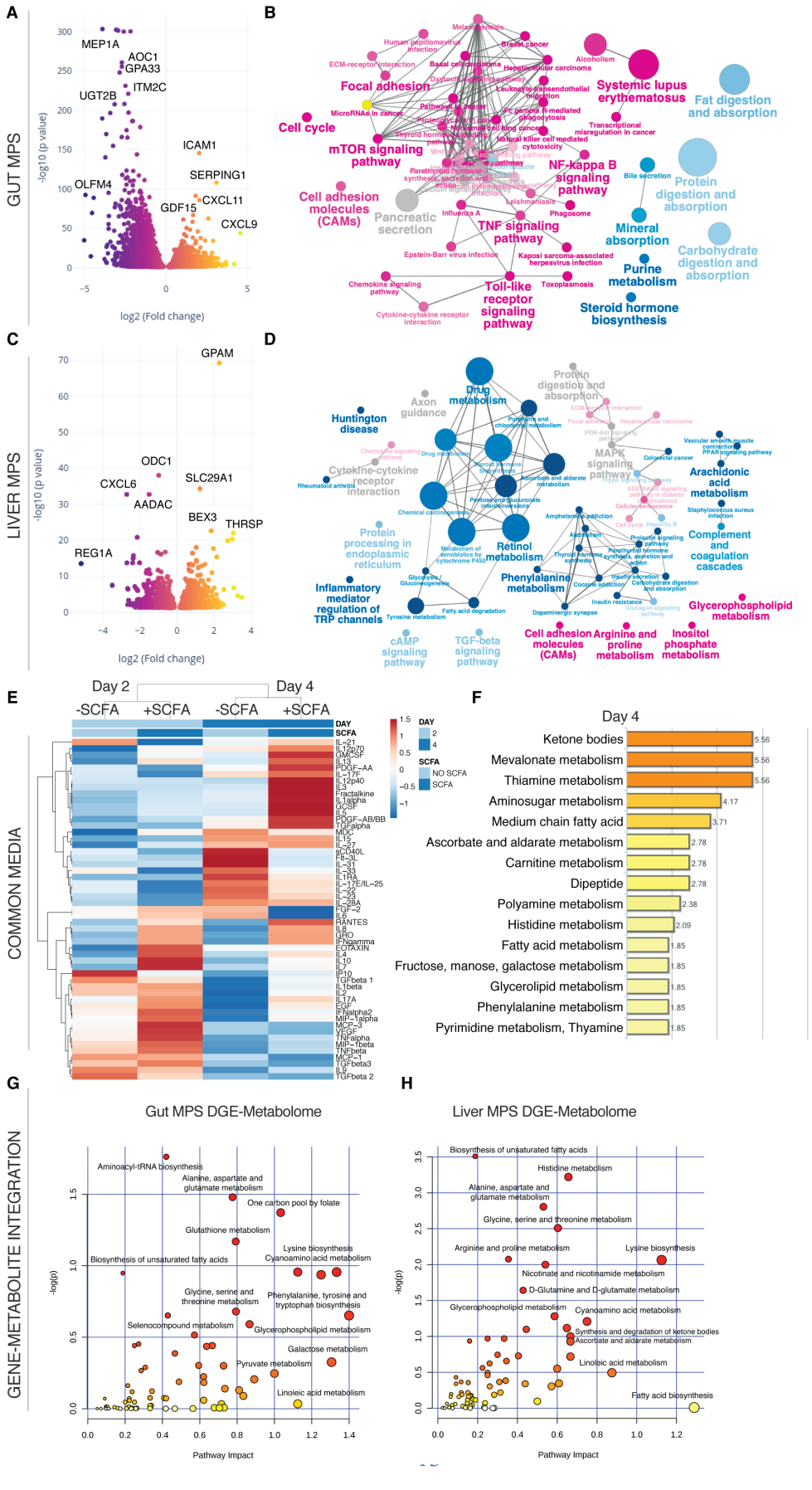

Fig.5 T cell mediated inflammation and tissue injury are significantly exacerbated by SCFA (A,C) Volcano plots of DEG in the gut MPSs (A) during interaction with the liver MPSs (C) and Treg/Th17 cells in presence or absence of SCFA. (B,D) Network of enriched (magenta) and downregulated (blue) pathways based on KEGG in gut MPSs (B) or liver MPSs (D). (E) Clustered heatmap of multiplexed cytokines/chemokines present in circulating common media at day 2 and 4 during gut-liver MPS interaction +/- SCFA. For actual concentrations of measured proteins and their importance consult Fig.S8. (F) Significantly enriched metabolic pathways based on quantification of metabolites found in the common medium at days 2 and 4 of gut-liver-SCFA interactions. (G,H) Integration of significantly upregulated genes in the UC gut MPSs (G) or liver MPSs (H) during interaction with Treg/Th17 cells and SCFA, and enriched metabolites found in the common medium at day 4. Pathway impact score is shown on the x-axis and statistical significance on the y-axis. All data represents 3 biological replicates.

SCFA act as inhibitors of HDAC and TRAF6 in activated CD4 T cells and stimulate Th1/Th2 differentiation with significant IL-13 production

SCFA have been previously shown in several studies to promote regulatory T cell development in the gut under steady-state conditions (*56*). However, during the gut-liver-SCFA interaction study, we showed SCFA to exacerbate acute inflammation upon the presence of CD4 effector T cells. These contradictory results led us to test the hypothesis that SCFA might affect CD4 T cells differently depending on their state of activation. We therefore performed an isolation study with the same 2:1 ratio of Treg to Th17 cells under steady-state and inflammatory conditions with SCFA. SCFA were added at an average concentration found in the common media (1 mM total) during the interaction study and at the physiological 7:2:1 ratio of acetate, propionate and butyrate. We stimulated human Treg/Th17 cells with IL-12/IFN-γ, which led to upregulation of inflammatory JAK-STAT and TNF pathways as well as to CD4 T cell specific differentiation into Th1/Th2 subtypes (Fig.6A). Next, we determined common and unique gene expressions comparing the 4 different groups; in the group of activated Treg/Th17 cells with SCFA, we identified 308 uniquely downregulated and 724 uniquely upregulated genes (Fig.6B).

Enrichment based on the REACTOME database indicated strong downregulation of HDAC activity, which has been shown in multiple studies (*57*), and p62-TRAF6 autophagy related pathways in activated, SCFA-treated CD4 T cells exclusively (Fig.6C). TRAF6 is an intrinsic T cell regulator required for immune homeostasis and its deletion leads to multiorgan inflammatory disease (*58*). Simultaneously, WNT activity and ECM receptor activity were increased in the same group (Fig. 6D). T cell activation pathways were significantly increased among stimulated and SCFA treated CD4 T cells, which is in line with a recent study on murine T cells (*59*). Moreover, SCFA were shown to inhibit FOXP3, the developmental gene required for Treg differentiation, thus dictating CD4 T cell effector versus tolerance phenotypes depending on the activation level of the cell (*21*). Specifically, both IL-10 and IL-13 cytokine-regulated extracellular protein pathways were increased as also seen during the interaction study with Treg/Th17 cells (Fig.S8).

Cytokine/chemokine measurements of their supernatants revealed stark differences among the groups (Fig.6E). Under steady state conditions addition of SCFA led to strongly increased TGF-β1 production consistent with previously published observations, in fact promoting tolerance. However, the trend seemed to be reversed in activated T cells, where SCFA led to increased release of IFN-γ, TNF-α and in particular IL-13, confirming the exacerbation potential of SCFA under inflammatory conditions. IL-13 is a critical promoter of UC and a target of interest in therapies against UC (*13*). Interestingly, regardless of activation state, SCFA prompted the higher release of the chemokines RANTES and MDC, which are important for additional recruitment of lymphocytes to sites of infection. Identifying the ability of SCFA to significantly increase IL-13 production by activated T cells and inhibit p62-TRAF6 activity is a novel finding with broad implication in understanding UC.

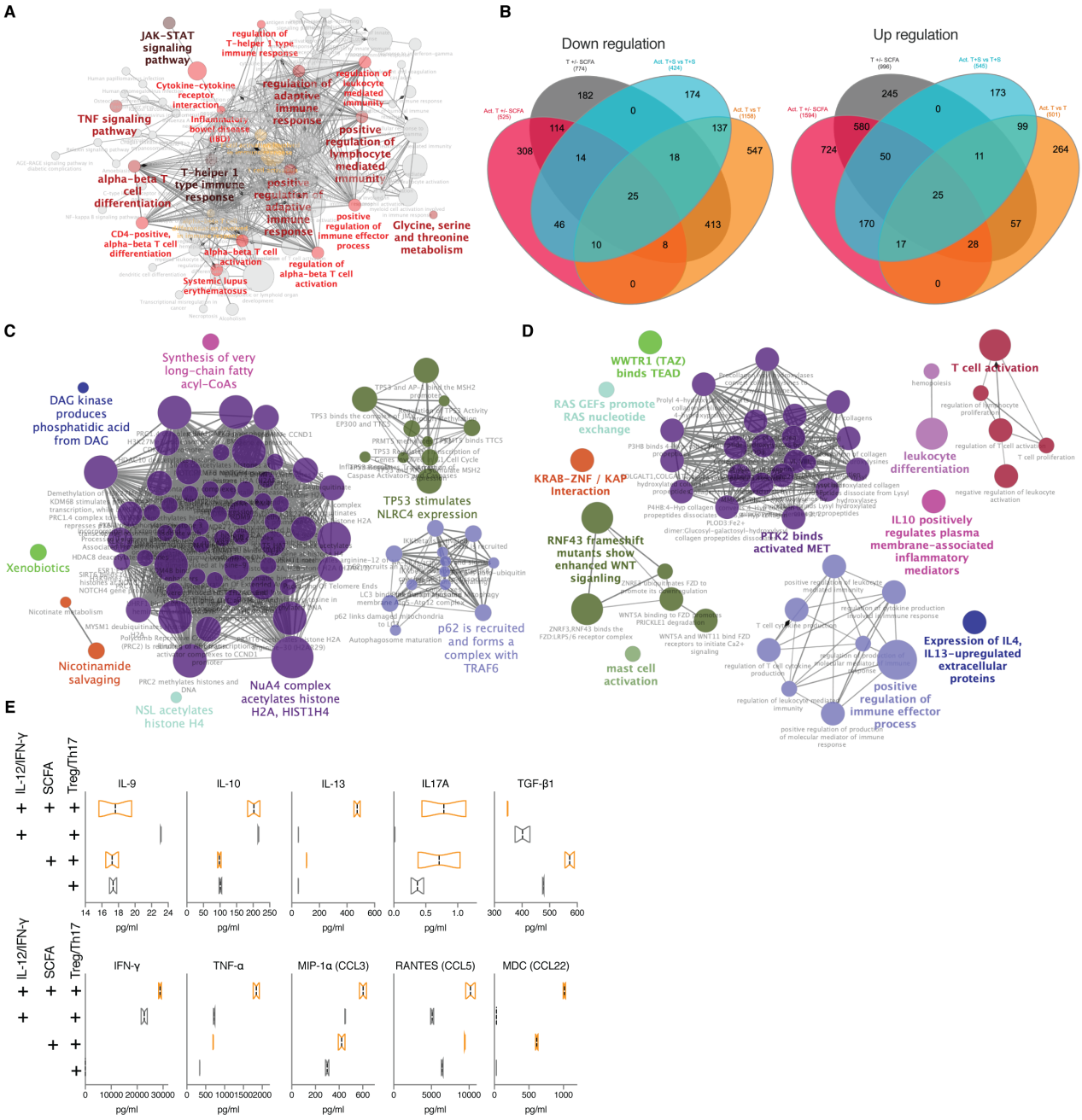

Fig.6 SCFA promote production of IL-13 and other inflammatory cytokines exclusively in activated T cells (A) Network of significantly enriched pathways based on KEGG in Treg/Th17 cells stimulated with IL-12 and IFN-γ (B) Venn diagram showing shared and unique significantly downregulated (left) or upregulated (right) genes among IL-12/IFN-γ stimulated Treg/Th17 cells +/- 1mM of total SCFA (magenta), unstimulated Treg/Th17 cells +/- 1mM of total SCFA (grey), IL-12/IFN-γ stimulated Treg/Th17 cells with SCFA over unstimulated T cells with SCFA (cyan), IL-12/IFN-γ stimulated Treg/Th17 cells over unstimulated T cells (orange). (C,D) Representative networks of downregulated pathways (C) or upregulated pathways (D) enriched based on REACTOME exclusively in IL-12/IFN-γ stimulated Treg/Th17 cells treated with 1mM of total SCFA. RNAseq analysis was performed on pooled cells from 3 independent experiments. (E) Multiplexed cytokines/chemokines in supernatants collected from each stimulated or unstimulated group with or without SCFA after 48 h of incubation.

Conclusion

By including Treg/Th17 cells in the interaction between the UC gut MPSs and liver MPSs, we recapitulated acute inflammatory conditions and global metabolomic changes described in advanced UC with concurrent autoimmune hepatic disease. While the mismatch between donors of individual cell types used in the study represents a clear technical limitation, we do believe the system to accurately represent the human biological CD4 T cell response, especially due to known disease parallels between alloimmunity, IBD or autoimmune liver diseases (*60, 61*). The gut MPS-induced CD4 T cell-mediated acute inflammation allowed us to probe temporal interconnectedness of microbiome-derived SCFA, innate and adoptive immune response without the use of xenopeptides to induce autoreactivity or chemicals, routinely used in animal models of IBD and autoimmune hepatitis (*62-64*). However, further advances in hiPSC and other technologies will allow us to recreate donor-matched physiomimetic experiments in the future, to which this current study represents an important stepping stone.

In partial agreement with previously published data, we were able to confirm SCFA to exert wide-ranging modifications of human gut and liver function, in part through actions on the innate and adaptive immune systems. SCFA appear to decrease innate immune activation of the ulcerative colitis gut MPS through PPAR signaling and downregulation of the NF-kappa B pathway (Fig.1-3). Reduced inflammation of the gut MPS favorably affected the gut-liver axis with increased hepatic metabolic function where conversion of SCFA lead to increased bile acid production, gluconeogenesis, lipid metabolism and formation of ketone bodies (Fig. 3). Under this condition and in contrast to common belief, SCFA gravely exacerbated CD4 T effector cell activation and liver injury. This was largely dependent on the direct influence of SCFA on activated Treg/Th17 cells through HDAC and p62-TRAF6 inhibition, metabolic reprograming and increased differentiation towards Th1/Th2 effector cells. At the same time, SCFA did promote Treg differentiation and production of TGF- β in non-stimulated Treg/Th17 populations as previously reported. Moreover, we have discovered the ability of SCFA to strongly increase the production of IL-13, a cytokine tightly connected to severity and progression of UC in humans. Cumulatively, these findings indicate that the role of SCFA greatly depends on the activation state of receptive CD4 T cells. While SCFA reduce innate immune activation of primary tissue in the absence of acute T cell inflammation, such as during early stages of UC, they might exert opposing effects in progressed acute UC with negative consequences for the hepatobiliary system. Activated, highly proliferative T cells largely require glucose for a robust response while resting immune cells switch fuel usage from glucose to fatty acids and ketones in support of tissue-protective pathways (*65*). However, SCFA and increased production of ketone bodies measured during interaction studies, further increased T cell effector function. This indicates that internal lymphocyte metabolic reprograming might not be as black and white, and that both anabolic and catabolic metabolic programs are potentially engaged concurrently which should be further explored. Our findings might explain in part the plethora of conflicting reports on the effects of SCFA in autoimmune/autoinflammatory diseases where their action seems to be highly context dependent.

Recreating hallmarks of human innate and adaptive immune mechanics of the gut-liver axis, although in absence of gut microbes, highlights the unique potential of human physiomimetic technologies to fill in the gaps in studying complex diseases through mechanistic correlation of various multiomic observations and systems immunology to both human and animal clinical data.

References

1. T. T. Macdonald, G. Monteleone, Immunity, inflammation, and allergy in the gut. *Science* **307**, 1920-1925 (2005).
2. D. H. Adams, B. Eksteen, Aberrant homing of mucosal T cells and extra-intestinal manifestations of inflammatory bowel disease. *Nat Rev Immunol* **6**, 244-251 (2006).
3. E. V. Loftus, Jr. *et al.*, PSC-IBD: a unique form of inflammatory bowel disease associated with primary sclerosing cholangitis. *Gut* **54**, 91-96 (2005).
4. D. K. Podolsky, Inflammatory bowel disease (2). *N Engl J Med* **325**, 1008-1016 (1991).
5. V. J. Desmet, M. Gerber, J. H. Hoofnagle, M. Manns, P. J. Scheuer, Classification of chronic hepatitis: diagnosis, grading and staging. *Hepatology* **19**, 1513-1520 (1994).
6. A. Y. Rudensky, Regulatory T cells and Foxp3. *Immunol Rev* **241**, 260-268 (2011).
7. Ivanov, II *et al.*, Induction of intestinal Th17 cells by segmented filamentous bacteria. *Cell* **139**, 485-498 (2009).
8. L. Zhou, G. F. Sonnenberg, Essential immunologic orchestrators of intestinal homeostasis. *Sci Immunol* **3**, (2018).
9. N. Eastaff-Leung, N. Mabarrack, A. Barbour, A. Cummins, S. Barry, Foxp3+ regulatory T cells, Th17 effector cells, and cytokine environment in inflammatory bowel disease. *J Clin Immunol* **30**, 80-89 (2010).
10. T. T. Feng, T. Zou, X. Wang, W. F. Zhao, A. L. Qin, Clinical significance of changes in the Th17/Treg ratio in autoimmune liver disease. *World J Gastroenterol* **23**, 3832-3838 (2017).
11. J. Wu *et al.*, Ablation of Transcription Factor IRF4 Promotes Transplant Acceptance by Driving Allogenic CD4(+) T Cell Dysfunction. *Immunity* **47**, 1114-1128 e1116 (2017).
12. I. J. Fuss *et al.*, Disparate CD4+ lamina propria (LP) lymphokine secretion profiles in inflammatory bowel disease. Crohn's disease LP cells manifest increased secretion of IFN-gamma, whereas ulcerative colitis LP cells manifest increased secretion of IL-5. *J Immunol* **157**, 1261-1270 (1996).
13. J. C. Hoving, Targeting IL-13 as a Host-Directed Therapy Against Ulcerative Colitis. *Front Cell Infect Mi* **8**, (2018).
14. S. Lavoie *et al.*, The Crohn's disease polymorphism, ATG16L1 T300A, alters the gut microbiota and enhances the local Th1/Th17 response. *Elife* **8**, (2019).
15. A. Koh, F. De Vadder, P. Kovatcheva-Datchary, F. Backhed, From Dietary Fiber to Host Physiology: Short-Chain Fatty Acids as Key Bacterial Metabolites. *Cell* **165**, 1332-1345 (2016).
16. A. N. Ananthakrishnan *et al.*, A prospective study of long-term intake of dietary fiber and risk of Crohn's disease and ulcerative colitis. *Gastroenterology* **145**, 970-977 (2013).
17. T. R. Sampson *et al.*, Gut Microbiota Regulate Motor Deficits and Neuroinflammation in a Model of Parkinson's Disease. *Cell* **167**, 1469-1480 e1412 (2016).
18. P. V. Chang, L. Hao, S. Offermanns, R. Medzhitov, The microbial metabolite butyrate regulates intestinal macrophage function via histone deacetylase inhibition. *Proc Natl Acad Sci U S A* **111**, 2247-2252 (2014).
19. M. Kespohl *et al.*, The Microbial Metabolite Butyrate Induces Expression of Th1-Associated Factors in CD4(+) T Cells. *Front Immunol* **8**, 1036 (2017).
20. J. Park, C. J. Goergen, H. HogenEsch, C. H. Kim, Chronically Elevated Levels of Short-Chain Fatty Acids Induce T Cell-Mediated Ureteritis and Hydronephrosis. *J Immunol* **196**, 2388-2400 (2016).
21. J. Park *et al.*, Short-chain fatty acids induce both effector and regulatory T cells by suppression of histone deacetylases and regulation of the mTOR-S6K pathway. *Mucosal Immunology* **8**, 80-93 (2015).
22. A. Trompette *et al.*, Dietary Fiber Confers Protection against Flu by Shaping Ly6c(-) Patrolling Monocyte Hematopoiesis and CD8(+) T Cell Metabolism. *Immunity* **48**, 992-1005 e1008 (2018).
23. M. Luu *et al.*, Regulation of the effector function of CD8(+) T cells by gut microbiota-derived metabolite butyrate. *Sci Rep-Uk* **8**, (2018).
24. R. I. Breuer *et al.*, Short chain fatty acid rectal irrigation for left-sided ulcerative colitis: a randomised, placebo controlled trial. *Gut* **40**, 485-491 (1997).
25. N. P. West *et al.*, Butyrylated starch increases colonic butyrate concentration but has limited effects on immunity in healthy physically active individuals. *Exerc Immunol Rev* **19**, 102-119 (2013).

26. A. L. Tarrerias *et al.*, Short-chain fatty acid enemas fail to decrease colonic hypersensitivity and inflammation in TNBS-induced colonic inflammation in rats. *Pain* **100**, 91-97 (2002).
27. B. E. Berndt *et al.*, Butyrate increases IL-23 production by stimulated dendritic cells. *Am J Physiol Gastrointest Liver Physiol* **303**, G1384-1392 (2012).
28. K. Ronaldson-Bouchard, G. Vunjak-Novakovic, Organs-on-a-Chip: A Fast Track for Engineered Human Tissues in Drug Development. *Cell Stem Cell* **22**, 310-324 (2018).
29. C. D. Edington *et al.*, Interconnected Microphysiological Systems for Quantitative Biology and Pharmacology Studies. *Sci Rep* **8**, 4530 (2018).
30. N. Tsamandouras *et al.*, Integrated Gut and Liver Microphysiological Systems for Quantitative In Vitro Pharmacokinetic Studies. *AAPS J* **19**, 1499-1512 (2017).
31. W. L. K. Chen *et al.*, Integrated gut/liver microphysiological systems elucidates inflammatory inter-tissue crosstalk. *Biotechnol Bioeng* **114**, 2648-2659 (2017).
32. T. C. DeRoche, S. Y. Xiao, X. Liu, Histological evaluation in ulcerative colitis. *Gastroenterol Rep (Oxf)* **2**, 178-192 (2014).
33. J. Kinchen *et al.*, Structural Remodeling of the Human Colonic Mesenchyme in Inflammatory Bowel Disease. *Cell* **175**, 372-+ (2018).
34. M. Barr, K. Gately, K. O'Byrne, Vascular endothelial growth factor (VEGF) is an autocrine survival factor in non-small cell lung cancer. *Lung Cancer* **75**, S2-S2 (2012).
35. J. H. Cummings, E. W. Pomare, W. J. Branch, C. P. Naylor, G. T. Macfarlane, Short chain fatty acids in human large intestine, portal, hepatic and venous blood. *Gut* **28**, 1221-1227 (1987).
36. P. Puchalska, P. A. Crawford, Multi-dimensional Roles of Ketone Bodies in Fuel Metabolism, Signaling, and Therapeutics. *Cell Metab* **25**, 262-284 (2017).
37. S. J. D. O'Keefe, Diet, microorganisms and their metabolites, and colon cancer. *Nat Rev Gastro Hepat* **13**, 691-706 (2016).
38. G. E. Kaiko *et al.*, The Colonic Crypt Protects Stem Cells from Microbiota-Derived Metabolites. *Cell* **167**, 1137 (2016).
39. E. Cholongitas *et al.*, Risk factors for recurrence of primary sclerosing cholangitis after liver transplantation. *Liver Transpl* **14**, 138-143 (2008).
40. B. Srinivasan *et al.*, TEER measurement techniques for in vitro barrier model systems. *J Lab Autom* **20**, 107-126 (2015).
41. D. J. Morrison, T. Preston, Formation of short chain fatty acids by the gut microbiota and their impact on human metabolism. *Gut Microbes* **7**, 189-200 (2016).
42. I. Kimura *et al.*, Short-chain fatty acids and ketones directly regulate sympathetic nervous system via G protein-coupled receptor 41 (GPR41). *Proc Natl Acad Sci U S A* **108**, 8030-8035 (2011).
43. S. J. Henning, F. J. Hird, Ketogenesis from butyrate and acetate by the caecum and the colon of rabbits. *Biochem J* **130**, 785-790 (1972).
44. G. Yan, L. Li, B. Zhu, Y. Li, Lipidome in colorectal cancer. *Oncotarget* **7**, 33429-33439 (2016).
45. B. Khor, A. Gardet, R. J. Xavier, Genetics and pathogenesis of inflammatory bowel disease. *Nature* **474**, 307-317 (2011).
46. M. Murai *et al.*, Peyer's patch is the essential site in initiating murine acute and lethal graft-versus-host reaction. *Nat Immunol* **4**, 154-160 (2003).
47. R. Perdigoto, H. A. Carpenter, A. J. Czaja, Frequency and significance of chronic ulcerative colitis in severe corticosteroid-treated autoimmune hepatitis. *J Hepatol* **14**, 325-331 (1992).
48. J. M. Griffin, K. M. Gilbert, L. W. Lamps, N. R. Pumford, CD4(+) T-cell activation and induction of autoimmune hepatitis following trichloroethylene treatment in MRL+/+ mice. *Toxicol Sci* **57**, 345-352 (2000).
49. R. L. Gieseck, 3rd, M. S. Wilson, T. A. Wynn, Type 2 immunity in tissue repair and fibrosis. *Nat Rev Immunol* **18**, 62-76 (2018).
50. H. K. Eltzschig, M. V. Sitkovsky, S. C. Robson, Purinergic signaling during inflammation. *N Engl J Med* **368**, 1260 (2013).
51. D. Okin, R. Medzhitov, The Effect of Sustained Inflammation on Hepatic Mevalonate Pathway Results in Hyperglycemia. *Cell* **165**, 343-356 (2016).
52. J. S. Lian *et al.*, A serum metabolomic analysis for diagnosis and biomarker discovery of primary biliary cirrhosis and autoimmune hepatitis. *Hepatobiliary Pancreat Dis Int* **14**, 413-421 (2015).
53. G. Kleiner *et al.*, Pediatric patients with inflammatory bowel disease exhibit increased serum levels of proinflammatory cytokines and chemokines, but decreased circulating levels of

macrophage inhibitory protein-1beta, interleukin-2 and interleukin-17. *Exp Ther Med* **9**, 2047-2052 (2015).
54. M. Maeda *et al.*, Serum tumor necrosis factor activity in inflammatory bowel disease. *Immunopharmacol Immunotoxicol* **14**, 451-461 (1992).
55. E. Roth *et al.*, Regulative potential of glutamine - Relation to glutathione metabolism. *Nutrition* **18**, 217-221 (2002).
56. P. M. Smith *et al.*, The microbial metabolites, short-chain fatty acids, regulate colonic Treg cell homeostasis. *Science* **341**, 569-573 (2013).
57. Y. Furusawa *et al.*, Commensal microbe-derived butyrate induces the differentiation of colonic regulatory T cells. *Nature* **504**, 446-450 (2013).
58. C. G. King *et al.*, TRAF6 is a T cell-intrinsic negative regulator required for the maintenance of immune homeostasis. *Nat Med* **12**, 1088-1092 (2006).
59. M. H. Kim, S. G. Kang, J. H. Park, M. Yanagisawa, C. H. Kim, Short-chain fatty acids activate GPR41 and GPR43 on intestinal epithelial cells to promote inflammatory responses in mice. *Gastroenterology* **145**, 396-406 e391-310 (2013).
60. L. Belyayev, K. Loh, T. M. Fishbein, A. Kroemer, The parallel paradigm between intestinal transplant inflammation and inflammatory bowel disease. *Curr Opin Organ Tran* **24**, 207-211 (2019).
61. M. Carbone, J. M. Neuberger, Autoimmune liver disease, autoimmunity and liver transplantation. *J Hepatol* **60**, 210-223 (2014).
62. Y. Liu *et al.*, Animal models of chronic liver diseases. *Am J Physiol Gastrointest Liver Physiol* **304**, G449-468 (2013).
63. V. Taneja, C. S. David, Lessons from animal models for human autoimmune diseases. *Nat Immunol* **2**, 781-784 (2001).
64. U. Erben *et al.*, A guide to histomorphological evaluation of intestinal inflammation in mouse models. *Int J Clin Exp Pathol* **7**, 4557-4576 (2014).
65. A. Wang, H. H. Luan, R. Medzhitov, An evolutionary perspective on immunometabolism. *Science* **363**, (2019).
66. M. Kasendra *et al.*, Development of a primary human Small Intestine-on-a-Chip using biopsy-derived organoids. *Sci Rep* **8**, 2871 (2018).
67. J. Roper *et al.*, In vivo genome editing and organoid transplantation models of colorectal cancer and metastasis. *Nat Biotechnol* **35**, 569-576 (2017).
68. U. Sarkar *et al.*, Metabolite profiling and pharmacokinetic evaluation of hydrocortisone in a perfused three-dimensional human liver bioreactor. *Drug Metab Dispos* **43**, 1091-1099 (2015).
69. T. J. Long *et al.*, Modeling Therapeutic Antibody-Small Molecule Drug-Drug Interactions Using a Three-Dimensional Perfusable Human Liver Coculture Platform. *Drug Metab Dispos* **44**, 1940-1948 (2016).
70. A. M. Clark *et al.*, A liver microphysiological system of tumor cell dormancy and inflammatory responsiveness is affected by scaffold properties. *Lab Chip* **17**, 156-168 (2016).
71. P. Ratajczak *et al.*, Th17/Treg ratio in human graft-versus-host disease. *Blood* **116**, 1165-1171 (2010).
72. T. Metsalu, J. Vilo, ClustVis: a web tool for visualizing clustering of multivariate data using Principal Component Analysis and heatmap. *Nucleic Acids Res* **43**, W566-570 (2015).
73. B. B. Evans AM, Liu Q, Mitchell MW, Robinson RJ, et al., High Resolution Mass Spectrometry Improves Data Quantity and Quality as Compared to Unit Mass Resolution Mass Spectrometry in High-Throughput Profiling Metabolomics. *Metabolomics* **4**, (2014).
74. A. R. Quinlan, I. M. Hall, BEDTools: a flexible suite of utilities for comparing genomic features. *Bioinformatics* **26**, 841-842 (2010).
75. A. Dobin *et al.*, STAR: ultrafast universal RNA-seq aligner. *Bioinformatics* **29**, 15-21 (2013).
76. B. Li, C. N. Dewey, RSEM: accurate transcript quantification from RNA-Seq data with or without a reference genome. *BMC Bioinformatics* **12**, 323 (2011).
77. M. I. Love, W. Huber, S. Anders, Moderated estimation of fold change and dispersion for RNA-seq data with DESeq2. *Genome Biol* **15**, 550 (2014).
78. A. Subramanian *et al.*, Gene set enrichment analysis: a knowledge-based approach for interpreting genome-wide expression profiles. *Proc Natl Acad Sci U S A* **102**, 15545-15550 (2005).

79. M. V. Kuleshov *et al.*, Enrichr: a comprehensive gene set enrichment analysis web server 2016 update. *Nucleic Acids Res* **44**, W90-97 (2016).
80. G. Bindea *et al.*, ClueGO: a Cytoscape plug-in to decipher functionally grouped gene ontology and pathway annotation networks. *Bioinformatics* **25**, 1091-1093 (2009).
81. J. Chong *et al.*, MetaboAnalyst 4.0: towards more transparent and integrative metabolomics analysis. *Nucleic Acids Res* **46**, W486-W494 (2018).

Acknowledgments: The authors are grateful to D Lauffenburger, O Yilmaz, S Mazmanian, A Wells for their critical input; to B Ringeisen, D Stepp, R Cecil and G Kost for their support and feedback; to O Yilmez, D Breault, G Eng, F Zhou, J Papps and V Hernandez-Gordillo for their help with establishing intestinal organoid cultures; V Butty, S Levine, D Brubaker and J Das for their help with RNAseq analysis and data representation; to JW Kemmitt for his help in operating the physiomimetic platforms and H Lee for managing lab operations **Funding:** DARPA W911NF-12-2-0039; NIH/NIBIB R01EB021908. **Author contributions:** MT, CC, DT and LG were responsible for conceptualization, investigation, data curation and analysis, methodology, visualization, and writing and review. MT, JV, CAM, YH, KS, CWW performed the experiments and assisted with data analysis; **Competing interests:** Authors declare no competing interests; **Data and materials availability:** Raw data and materials can be obtained by inquiry to the authors.

Supplementary Materials:

Figures S1-S9

Table S1

References (*64-81*)